JAAS

Journal of Analytical Atomic Spectrometry

www.rsc.org/jaas

Volume 26 | Number 4 | April 2011 | Pages 637–872

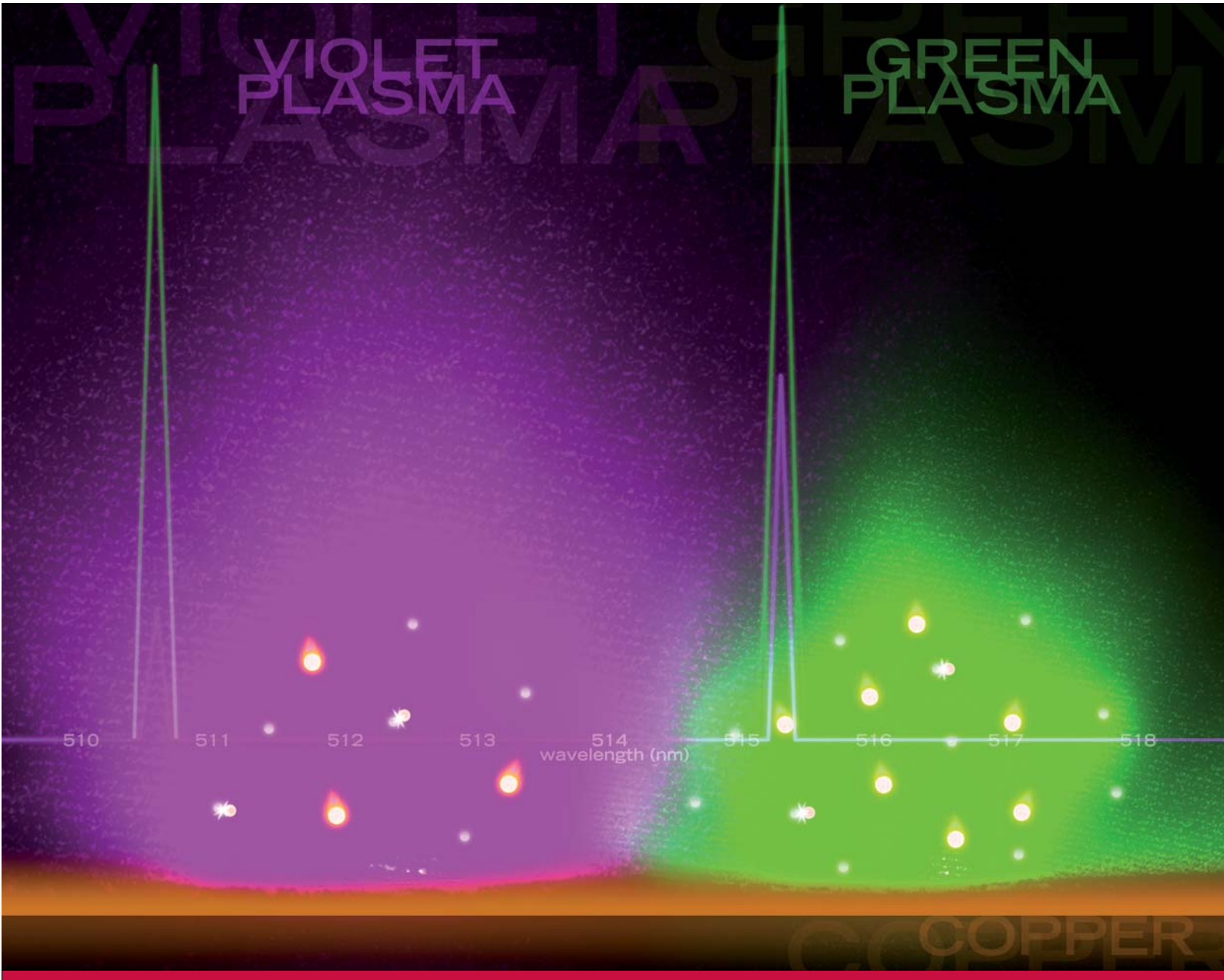

Themed Issue: Glow Discharge Spectroscopy

ISSN 0267-9477

RSC Publishing

PAPER

Bordel *et al.*

Spatial characterization of pressure-based plasma regimes in a radiofrequency glow discharge by using optical emission spectroscopy

2011 CHEMISTRY

International Year of CHEMISTRY 2011

0267-9477(2011)26:4;1-A

Spatial characterization of pressure-based plasma regimes in a radiofrequency glow discharge by using optical emission spectroscopy†‡

Rebeca Valledor,[a] Jorge Pisonero,[a] Thomas Nelis§[b] and Nerea Bordel*[a]

Received 1st October 2010, Accepted 5th November 2010
DOI: 10.1039/c0ja00177e

A new experimental set-up has been developed in order to perform spatially resolved measurements of the optical emission in a radiofrequency glow discharge (rf-GD). The emitted radiation is not only detected through an end-on window (as usually done in commercial GD-OES instruments), but the emission along the plasma plume is also measured axially-resolved by side-on measurements. The GD source is a modified Grimm-type source and follows a previous configuration designed for analytical applications in glow discharge coupled to mass spectrometry (GD-MS) instruments. Depending on the argon flow rate and pressure, and for a pure copper sample, two different plasma regimes have been observed and characterized by analyzing the spatial distribution of different excited species present in the plasma. Keeping a constant Ar flow rate, pressures higher than a certain value lead to enhanced Cu (analyte) emission (green regime) while at lower pressures a violet plasma is observed. In the violet regime, the spatial extension of Cu and Ar excited species along the plasma axis is found to be broader.

Introduction

Glow discharge (GD) atomic spectrometric techniques, such as glow discharge mass spectrometry (GD-MS) and glow discharge optical emission spectrometry (GD-OES), are commonly used as analytical methods able to provide fast and sensitive direct chemical analysis as well as high resolved depth profile analysis of coated materials.[1–6]

Traditionally, GD-OES instruments allow end-on view of the GD plasma, the emission spectra being collected with a point-focused lens and integrated over the whole plasma. Spatially resolved measurements of the spectral emission of the sample surface could be achieved using imaging spectrometers. In this sense, several studies have been performed using pulsed radio-frequency glow discharge (pulsed-rf-GD). For instance, Zenitani and Wagatsuma[7] found that parameters such as electron density and temperature are not uniform in the plasma, but change along the radial direction. Additionally, Gamez *et al.*[8] developed an instrument for three dimensional imaging that could be applied to qualitative and quantitative analysis of conducting and non-conducting samples.

The observation of the GD plasma plume along its axis (side-on instead of end-on viewing) can provide useful information on the spatial distribution of the different excited/ionized species, since different discharge processes could take place at different distances from the sample. For instance, the knowledge of the ion population distribution could be useful to optimize the positioning of a sampler cone to couple the GD source to a mass spectrometer. One of the first studies of the emission in a glow discharge with side-on detection was performed by Dogan *et al.*[9] In particular, they investigated the more important physical properties of a Grimm glow discharge lamp. However, most of the spatially resolved studies have been performed with direct insertion probe GD sources. Hoppstock and Harrison[10] studied the spatial distribution of copper and argon in a direct current glow discharge (discharge current of 4 mA and discharge voltage of ~1000 V), by atomic emission and absorption spectrometry. They found, at a pressure of 133 Pa, that the emission and absorbance profiles of the atomic species showed a maximum at a distance of 0.75–1 mm from the sample surface, while ion emission only increased in front of the center of the cathode. A similar study was carried out by Rozsa *et al.*,[11] who found that atomic argon emission peaked at a similar distance (0.8–1 mm from the cathode surface). This area was identified as the cathode glow region. A second maximum appeared at a distance between 6 and 15 mm from the cathode surface, depending on the current intensity (0.25–8 mA) and pressure (13–67 Pa). This area was identified as the negative glow region. In contrast, ionic argon emission only showed a single maximum placed in the negative glow. In this study (performed at considerably lower pressure than that in our work) it was demonstrated that Ar excited species were extended more than 40 mm from the cathode surface. More recently, Jackson *et al.*[12] and Lewis *et al.*[13] studied not only the spatial but also the temporal characteristics of a pulsed GD, by atomic emission, atomic absorption and laser induced fluorescence measurements, using a frequency of 50 Hz, a duty cycle of 25% and a pressure of 106 Pa. They investigated the Ar metastable production and the copper analyte excitation and ionization processes to find out that the spatial position for the highest analyte population depends on the temporal region

[a]*Department of Physics, University of Oviedo, 33600 Mieres, Spain. E-mail: bordel@uniovi.es*
[b]*LAPLACE, Université Paul Sabatier, 118 rte de Narbonne, Bat3R2, 31062 Toulouse Cedex, France*

† This article is part of a themed issue highlighting the latest work in the area of Glow Discharge Spectroscopy, including the work presented at the International Glow Discharge Spectroscopy Symposium 2010, August 22–25, Albi, France.

‡ Electronic supplementary information (ESI) available: Photo of the GD experimental set-up and the optics used to perform the spatially resolved side-on measurements. See DOI: 10.1039/c0ja00177e

§ Present address: CUFR Jean François Champollion, 81000 Albi, France.

along the GD pulse and also on the energy levels involved in the transitions.

The direct insertion probe GD configuration presents problems such as redeposition on source components and thermal effects.[14] In contrast, the use of a Grimm-type source allows the external mounting of the sample, and defines the sputtered area providing the possibility of depth profiling. Traditionally, direct insertion probe GD has been the most employed in GD-MS instruments; however, nowadays there are commercial GD-MS instruments, in addition to the GD-OES, that utilize the Grimm-type source. To carry out spatially resolved measurements in this type of GD sources is a rather difficult task due to the electrodes disposition (tenths of mm between sample and anode) and to the anode shape (cylindrical), if no modification of the design is done. In this sense Smid *et al.* used a modified Grimm-type dc powered GD source to study the effect of hydrogen on the spatial distribution of some iron and zinc emission lines.[15] The inner diameter of the anode tube was 8 mm, and it had a longitudinal slot used to record the emission spectra at 12 positions up to 7 mm from the cathode. They found that the intensity distribution of the iron lines was shifted closer to the cathode in the presence of hydrogen. All these earlier experimental results were obtained using discharge sources without significant gas flow in the discharge volume.

In the present work, the spatial distribution of argon and copper excited species is investigated along the plasma plume in a radiofrequency GD, which consists of a modified Grimm-type source, previously designed for analytical purposes.[16] One significant difference between this source and the sources used for earlier studies is the introduction of argon close to the cathode, thus introducing a gas flow through the discharge volume. The thickness of this GD source is of only 7 mm in order to detect the emission from points relatively close to the cathode. Emission spectra have been acquired at different GD operating conditions, being observed that for a selected argon flow rate, the emission characteristics change notoriously depending on the pressure. In fact, in some experiments previously performed with a GD-TOFMS instrument used in our laboratory, it had been already observed a sudden increase of the ionic analytical signal and a decrease of the Ar^+ intensity when closing the valve that regulates the pumping speed that could be related to the transition described in this work. Our studies have shown that increased pressure results in higher Cu intensities at positions close to the cathode. Moreover, the spatial extension of the Cu excited species was longer at lower Ar pressure, keeping a constant flow rate. The decay of Ar emission at increasing distances from the cathode is faster at higher pressures (constant flow rate).

Experimental

A new in-house GD source allowing spatially resolved measurements along the plasma plume was designed and built (Fig. 1). The GD anode follows a previous design developed by Pisonero *et al.* for analytical purposes.[16–18] It consists of a rectangular piece made of brass, having an internal cone with a 4 mm orifice diameter. The GD anode has one argon inlet, which is bifurcated inside the chamber into two inner channels (1.5 mm diameter) facing at the internal space of the anode. The argon

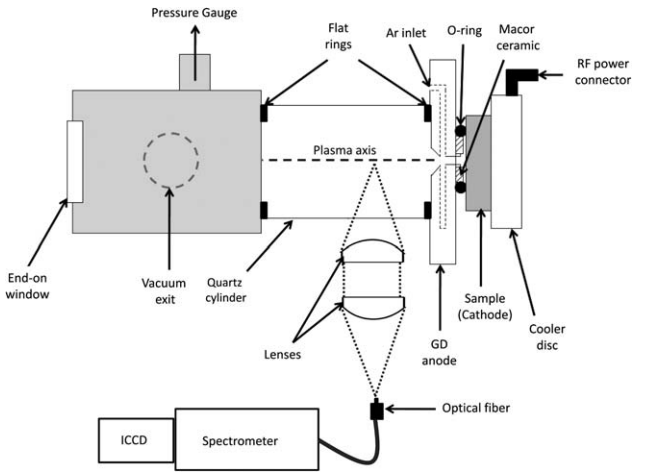

Fig. 1 Schematic diagram of the Grimm-type source developed in the laboratory.

flow rate was controlled with a mass flow controller (MKS Model 1179B). The sample was placed externally on one side of the GD anode, against a macor ceramic spacer and a sealing O-ring. The GD plasma was powered by a radiofrequency power supply (Dressler CESAR Generator Model 133, CO, USA) that provides up to 300 W as maximum output power. The reflected power was minimized by employing a matching network (Advanced Energy ATX Tuner, USA). On the other side of the anode, a quartz cylinder fits by means of a sealing flat ring. This quartz cylinder is transparent for visible and UV lights down to 200 nm. It thus allows side-on measurements of the plasma plume with axial resolution. Another flat seal was placed between the quartz cylinder and a metallic piece with cubic shape, which provides the system with two symmetric vacuum exits in the lateral sides and a third port to connect a pressure gauge (MKS Baratron capacitance pressure transducer, Model 122B) on the upper side. Moreover, this source has a frontal glass window to also allow end-on viewing, like in conventional GD-OES instruments.

The discharge chamber was pumped using a rotary pump (model Pascal 2010SD, Alcatel, France). Afterwards, Ar with 99.999% minimum purity (Air Liquide, Asturias, Spain) was introduced as discharge gas in the source. During discharge operation the pressure was kept constant at values between 450 and 720 Pa. The radiofrequency forward power applied in this work was 42 $\pm$ 1 W. The power supplied to the discharge is expected to be 20–30% lower.[19]

Minimizing the thickness of the source body was a key parameter for this work. The new source allows measuring the radiation emitted from points relatively close to the sample surface. In this work, the minimum real distance to the sample from which it is possible to collect radiation is of approximately 9 mm. This point has been chosen as the reference point and, thus, it will be defined as "0 mm lateral position" for simplicity.

The detection system consists of two flat-convex lenses that focus the radiation, which is emitted from the plasma plume, and goes through the quartz cylinder into an optical fiber (ref. LG-455-020-3). Both the lenses and the optical fiber are fixed to two movable supports which allow their movement along the plasma

Table 1 Cu and Ar transitions studied in this work

Element	λ/nm	$Energy_{lower\ level}$/eV	$Energy_{upper\ level}$/eV	Lower level	Upper level
Cu II	224.70	2.72	8.23	$3d^9 4s(^3D_3)$	$3d^9 4p(^3P^0_2)$
Cu I	222.57	0.00	5.57	$3d^{10} 4s(^2S_{1/2})$	$3d^9(^2D)4s4p(^3P^0)(^2F^0_{7/2})$
	222.78	1.64	7.21	$3d^9 4s^2(^2D_{3/2})$	$3d^9(^2D)4s4p(^1P^0)(^2F^0_{5/2})$
	223.01	1.39	6.95	$3d^9 4s^2(^2D_{5/2})$	$3d^9(^2D)4s4p(^1P^0)(^2F^0_{7/2})$
	224.43	0.00	5.52	$3d^{10} 4s(^2S_{1/2})$	$3d^9(^2D)4s4p(^3P^0)(^4D^0_{3/2})$
	282.44	1.39	5.78	$3d^9 4s^2(^2D_{5/2})$	$3d^9(^2D)4s4p(^3P^0)(^2D^0_{5/2})$
	324.75	0.00	3.82	$3d^{10} 4s(^2S_{1/2})$	$3d^{10} 4p(^2P^0_{3/2})$
	327.40	0.00	3.79	$3d^{10} 4s(^2S_{1/2})$	$3d^{10} 4p(^2P^0_{1/2})$
	327.98	1.64	5.42	$3d^9 4s^2(^2D_{5/2})$	$3d^9(^2D)4s4p(^3P^0)(^2F^0_{5/2})$
	333.78	1.39	5.10	$3d^9 4s^2(^2D_{5/2})$	$3d^9(^2D)4s4p(^3P^0)(^4F^0_{7/2})$
	365.42	3.79	7.18	$3d^{10} 4p(^2P^0_{1/2})$	$3d^{10} 6d(^2D_{3/2})$
	368.74	3.82	7.18	$3d^{10} 4p(^2P^0_{3/2})$	$3d^{10} 6d(^2D_{3/2})$
	510.55	1.39	3.82	$3d^9 4s^2(^2D_{5/2})$	$3d^{10} 4p(^2P^0_{3/2})$
	515.32	3.79	6.19	$3d^{10} 4p(^2P^0_{1/2})$	$3d^{10} 4d(^2D_{3/2})$
	521.82	3.82	6.19	$3d^{10} 4p(^2P^0_{3/2})$	$3d^{10} 4d(^2D_{5/2})$
Ar I	415.86	11.55	14.53	$3s^2 3p^5(^2P^0_{3/2})4s[3/2]^0_2$	$3s^2 3p^5(^2P^0_{3/2})5p[3/2]_2$
	418.19	11.72	14.69	$3s^2 3p^5(^2P^0_{1/2})4s[1/2]^0_0$	$3s^2 3p^5(^2P^0_{1/2})5p[1/2]_1$
	419.83	11.62	14.58	$3s^2 3p^5(^2P^0_{3/2})4s[3/2]^0_1$	$3s^2 3p^5(^2P^0_{3/2})5p[1/2]_0$
	420.07	11.55	14.50	$3s^2 3p^5(^2P^0_{3/2})4s[3/2]^0_2$	$3s^2 3p^5(^2P^0_{3/2})5p[5/2]_3$
	451.07	11.83	14.58	$3s^2 3p^5(^2P^0_{1/2})4s[1/2]^0_1$	$3s^2 3p^5(^2P^0_{3/2})5p[1/2]_0$
	452.23	11.72	14.46	$3s^2 3p^5(^2P^0_{1/2})4s[1/2]^0_0$	$3s^2 3p^5(^2P^0_{3/2})5p[1/2]_1$
	459.61	11.83	14.52	$3s^2 3p^5(^2P^0_{1/2})4s[1/2]^0_1$	$3s^2 3p^5(^2P^0_{3/2})5p[3/2]_1$
	470.23	11.83	14.46	$3s^2 3p^5(^2P^0_{1/2})4s[1/2]^0_1$	$3s^2 3p^5(^2P^0_{3/2})5p[1/2]_1$
	750.39	11.83	13.48	$3s^2 3p^5(^2P^0_{1/2})4s[1/2]^0_1$	$3s^2 3p^5(^2P^0_{1/2})4p[1/2]_0$
	751.47	11.62	13.27	$3s^2 3p^5(^2P^0_{3/2})4s[3/2]^0_1$	$3s^2 3p^5(^2P^0_{3/2})4p[1/2]_0$
	763.51	11.55	13.17	$3s^2 3p^5(^2P^0_{3/2})4s[3/2]^0_2$	$3s^2 3p^5(^2P^0_{3/2})4p[3/2]_2$
Ar II	410.39	19.49	22.51	$3s^2 3p^4(^3P)4p(^4D^0_{7/2})$	$3s^2 3p^4(^3P)5s(^4P_{5/2})$
	457.94	17.26	19.97	$3s^2 3p^4(^3P)4s(^2P_{1/2})$	$3s^2 3p^4(^3P)4p(^2S^0_{1/2})$
	459.88	18.66	21.35	$3s^2 3p^4(^3P)3d(^2D_{3/2})$	$3s^2 3p^4(^1D)4p(^2P^0_{3/2})$
	465.79	17.14	19.80	$3s^2 3p^4(^3P)4s(^2P_{3/2})$	$3s^2 3p^4(^3P)4p(^2P^0_{1/2})$

plume axis. The spatial resolution achieved for the side-on measurements was approximately 1 mm. The other edge of the optical fiber is fixed to the entrance slit of a 0.5 m spectrograph (SpectraProR-500, Princeton Instruments, NJ, USA), which can be operated using two ruled gratings of 2400 and 3600 lines mm^{-1}, respectively. The detector was an intensified charge coupled device (ICCD) (PI-MAX camera, ST-133 controller, Princeton Instruments, NJ, USA).

A 99.99% pure copper sample was used in this work (ref. 185-CP5, SPEX CertiPrep Ltd., UK). The sample surface was polished to a mirror finish using metallographic grinding papers (120, 600 and 1200 grit) and then cleaned with ethanol. The Ar and Cu transitions studied in this work are listed in Table 1.[20,21]

Crater profiles obtained after GD sputtering were measured with a profilometer (Perth-o-meter S6P, Mahr Perthen, Göttingen, Germany). The sputtering rates were calculated using the software "CraterVol".[22]

Results and discussion

Plasma regimes

Two different plasma appearances have been observed for the pure copper sample when operating the GD at certain argon flow rate and depending on the pressure conditions. It should be highlighted that in this experimental set-up it is possible to independently control the Ar flow rate and the pressure in the discharge source. In particular, carrier gas flow rate is selected using the mass flow controller, while the desired pressure is achieved regulating the pumping speed by means of a valve placed at the entrance of the rotary pump. When the pressure was increased at a fixed flow rate value, the dc-bias voltage decreased progressively. This decrease of dc-bias with increasing pressure is also observed in standard Grimm-type lamps with no significant gas flow in the discharge volume.[23] When the pressure reached a certain value, the plasma plume, violet at low pressure (according to the predominant argon emission around 400–420 nm) turned into a green color. This sudden change is accompanied by an enhancement of the copper emission (in particular, of the copper lines around 510 nm), and by an increase of the dc-bias by 15%. These sudden changes are not observed in standard Grimm lamps. Table 2 summarizes the plasma regimes/aspects observed at different operating conditions. The conditions at which the transition between the green and the violet plasma appears are not well defined. For instance, at 250 sccm and 600 Pa the plasma could be either violet or green. At these conditions when the plasma was violet, a dc-bias voltage of 315 V was measured, while this value suddenly increased up to 365 V when the plasma suffered the transition to the green regime.

Table 2 Plasma regimes as a function of argon flow rate and pressure

	Pressure/Pa		
Flow rate/sccm	500	600	700
250	Violet	Violet/green	Green
275	Violet	Violet/green	Green
300	Violet	Violet	Green

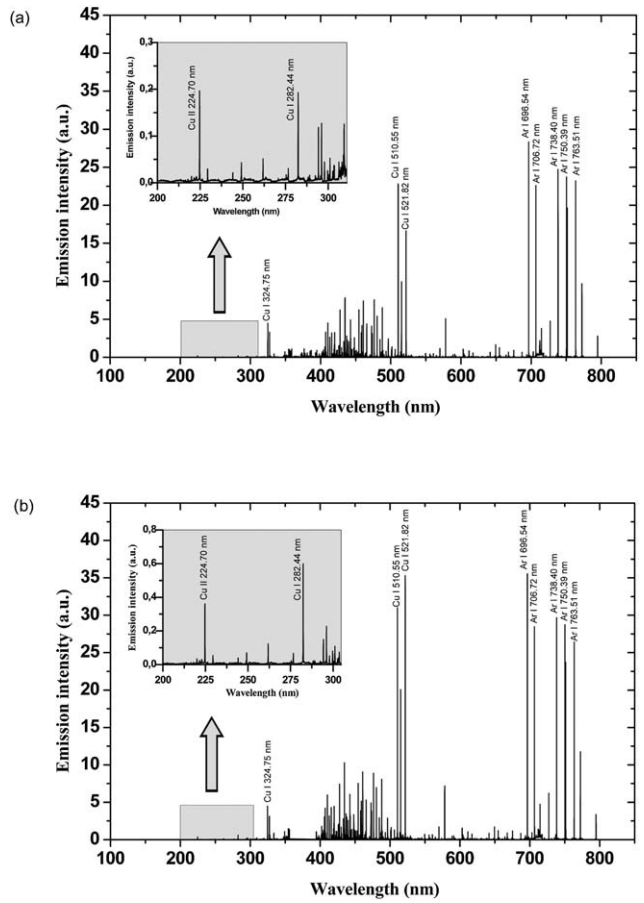

Fig. 2 On-axis emission spectra: (a) violet regime at 275 sccm, 560 Pa and 42 W; (b) green regime at 275 sccm, 720 Pa and 42 W.

On-axis measurements (end-on viewing)

Fig. 2 shows the emission spectra (from 200 to 800 nm) collected through the end-on window for both plasma regimes. Plasma transition was achieved varying the pressure (560 Pa for violet plasma and 720 Pa for green plasma) while keeping a constant applied power (42 W) and flow rate (275 sccm). Emission spectra are not corrected for the efficiency of the detection system (end-on glass window, optical fiber, spectrometer and ICCD). This efficiency, in particular the transmission of the glass window, is much lower in the ultraviolet region than in the visible part of the spectrum. This fact explains why the resonance Cu lines at 324.75 and 327.40 nm are not the most intense Cu lines observed in both spectra. The green regime (Fig. 2b) leads to higher emission intensities than in the violet plasma (Fig. 2a), and especially atomic non-resonance copper lines are enhanced in the green case. Additionally the most intense copper line in the green plasma is the 521.82 nm line, while in the violet plasma it is the 510.55 nm line. Table 3 lists the green to violet intensity ratio for several copper and argon lines. It is noticed that all the studied emission lines are enhanced in the green regime, except resonance lines at 324.75 nm and 327.40 nm, which decrease due to high self-absorption. The copper lines increase by a factor of 2–3, whereas the Ar emission increases by a factor of 1.0–1.4 only. This behavior justifies the change of color observed in the transition from one regime to the other.

Table 3 Green to violet intensity ratio for several copper and argon lines (on-axis measurements). The standard deviation of this ratio is about 10%

$\lambda_{Cu\ I}$/nm	I_{green}/I_{violet}	$\lambda_{Ar\ I}$/nm	I_{green}/I_{violet}	λ_{ionic}/nm	I_{green}/I_{violet}
222.57	2.05	415.86	1.32	224.70 (Cu II)	1.85
222.78	2.45	418.19	1.28	410.39 (Ar II)	1.00
223.01	2.01	419.83	1.31	459.88 (Ar II)	1.34
282.44	3.20	420.07	1.37	457.94 (Ar II)	1.18
324.75	0.99	451.07	1.24	465.79 (Ar II)	1.21
327.40	0.94	452.23	1.44		
327.98	2.65	459.61	1.38		
333.78	2.11	470.23	1.20		
365.42	1.62	750.39	1.21		
368.74	2.93	751.47	1.21		
510.55	1.36	763.51	1.02		
515.32	2.03				
521.82	2.07				

This effect might have been caused by an increase in the sputtering rate in the green plasma. To check this hypothesis, the sputtering rates were determined using a profilometer and the CraterVol software.[22] The values obtained demonstrated that the sputtering rate in the green plasma was only 1.2 times higher than in the violet regime. This result is in line with the behavior of a standard Grimm source. For this configuration, the sputtering depends almost linearly on the rf-power and little on the source impedance or pressure. The enhancement of the emission yield, emission intensity divided by sputtering rate, with increasing pressure is also in line with observation made using the Grimm source in end-on view. The sudden transition in the dc-bias, however, has not been observed in rf-Grimm sources.

Orthogonal to axis measurements (side-on viewing)

Emission spectra between 200 and 800 nm were also measured for both plasma regimes along the plasma plume axis. Fig. 3 shows the emission spectra collected through the quartz cylinder at 0 mm lateral position for both plasma regimes (keeping a constant flow rate of 275 sccm, the violet plasma was established at 550 Pa and the green regime at 720 Pa). It is observed that UV lines are the most intense lines, in contrast to previous observations in end-on viewing (see Fig. 2). The reason for this is that the optical system used for the side-on measurements has a better transmission at UV wavelengths (UV transmission through the quartz cylinder is higher than through the end-on glass window). Fig. 3a shows that the resonance copper lines are the most intense lines in the violet plasma, while an important enhancement of some other copper lines in the green regime (Fig. 3b) can be noticed.

The ratio of the line intensities measured in the green plasma to those measured in the violet plasma was calculated for the shortest distance to the cathode (0 mm reference distance) for most of the lines studied. The results are shown in Table 4. Comparing argon and copper ionic and atomic lines, we find significantly different behaviors: atomic argon lines have a similar emission in both regimes at the 0 mm reference distance, while ionic argon emission is clearly higher in the violet plasma. In contrast, all the copper lines are considerably enhanced in the green regime, since the intensity ratios take values between

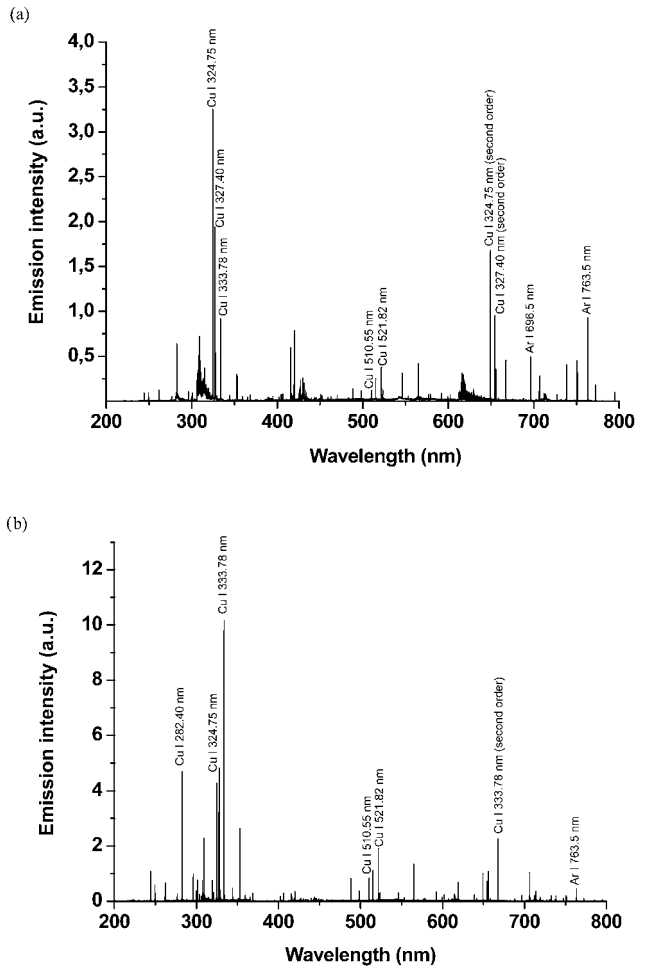

Fig. 3 Orthogonal to axis emission spectra (at 0 mm lateral position, really placed 9 mm far from the sample surface); (a) violet regime at 275 sccm, 550 Pa and 42 W; (b) green regime at 275 sccm, 720 Pa and 42 W.

3 and 8. The emission of resonance copper lines is the least enhanced in the green plasma. This copper emission enhancement explains why the plasma appearance changes to a green color when the regime transition occurs.

The spectrum taken in the green regime (see Fig. 3b) appears to be affected by stronger self-absorption compared to the violet regime. The intensity ratio between the two copper resonance lines at 324.75 nm and 327.40 nm is about 1.3 in the green regime and about 1.7 in the violet plasma. Without self-absorption a ratio of 2 between the two lines should be expected. The ratio between the emission intensity of the 324.75 nm line (resonance copper line) and the 510.55 nm line is higher in the violet plume (about 22) than in the green regime (about 4). As both lines originate from the same upper level, this ratio is expected to be around 70. Therefore, the ratios obtained also indicate less self-absorption in the violet plasma plume. The fact that the characteristic pair resonance lines represent the strongest lines in the violet regime, but in the green regime the non-resonance line at 333.78 nm is the strongest one, also hints in the same direction of enhanced self-absorption. The most likely interpretation of this difference in self-absorption is that the copper atom density is higher in the green plasma.

Table 4 Ratio between the intensity measured at the 0 mm reference position in the green regime and that measured in the violet regime, for several argon and copper lines

	Wavelength/nm	Energy$_{\text{upper level}}$/eV	$I_{\text{green}}/I_{\text{violet}}$
Cu II	224.70	8.23	5.0 ± 0.3
Cu I	222.57	5.57	7.8 ± 0.3
	222.78	7.21	7.0 ± 0.4
	223.01	6.95	6.7 ± 0.4
	224.43	5.52	8.1 ± 0.7
	282.44	5.78	5.2 ± 0.2
	324.75	3.82	2.9 ± 0.1
	327.40	3.79	3.1 ± 0.1
	327.98	5.42	5.8 ± 0.4
	333.78	5.10	7.9 ± 0.3
	365.42	7.18	5.9 ± 0.3
	368.74	7.18	6.1 ± 0.1
	510.55	3.82	8.5 ± 1.0
	515.32	6.19	5.1 ± 1.1
Ar II	459.88	21.35	0.9 ± 0.1
	457.94	19.97	0.38 ± 0.05
	465.79	19.80	0.45 ± 0.04
Ar I	418.19	14.69	1.0 ± 0.1
	419.83	14.58	1.04 ± 0.04
	451.07	14.58	0.91 ± 0.03
	415.86	14.53	1.11 ± 0.03
	459.61	14.52	1.04 ± 0.06
	420.07	14.50	1.14 ± 0.02
	470.23	14.46	1.25 ± 0.05
	452.23	14.46	0.99 ± 0.04
	750.39	13.48	1.17 ± 0.03
	751.47	13.27	1.17 ± 0.03
	763.51	13.17	1.09 ± 0.03

Spatially resolved studies

Further investigations on the distribution of the emission intensity with the distance to the sample surface were performed for some Cu and Ar emission lines in both plasma regimes. From the 0 mm lateral position (real distance to the sample ~9 mm), the optical system was moved along 10 mm parallel to the plasma plume axis in steps of 1 mm. The discharge conditions were similar to those used previously: forward power of 42 W, gas flow rate of 275 sccm, and pressures between 450 and 600 Pa for the violet plasma and between 600 and 720 Pa for the green plasma.

Copper emission. The spatial distribution of different atomic and ionic copper lines was analyzed. Fig. 4 shows the variation of the emission intensity along the plasma plume axis observed in the green and violet plasma for the atomic copper lines at 510.55 nm (Fig. 4a) and 515.32 nm (Fig. 4b). For both emission lines, the intensity in the green regime is clearly higher on the first millimetres studied, although it drops with the distance much faster than in the violet plasma. Additionally, it is observed that at 515.32 nm the emission signal decreases in the green regime so fast at further distances that it becomes even lower than in the violet plasma. To give a quantitative measure of how fast the intensity decreases, the distance at which the intensity has dropped to 20% of the maximum value was estimated. In the green plasma regime, this point is reached at about 7.0 mm for the 510.55 nm line and at 3.8 mm for the 515.32 nm line. In the violet regime, however, the signal does not reach this level within the zone of observation. After 10 mm the decrease is of only 27% for the 510.55 nm line and of 60% for the 515.32 nm line.

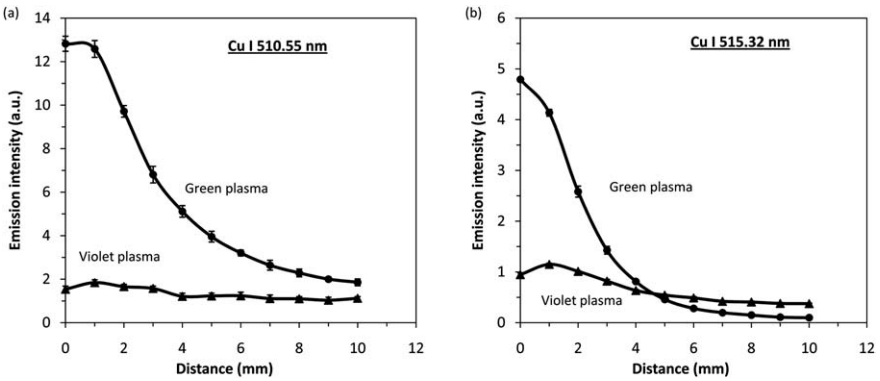

Fig. 4 Spatially resolved measurement of the atomic copper emission for both plasma regimes (violet plasma at 275 sccm, 500 Pa and 42 W (▲); and green plasma at 275 sccm, 600 Pa and 42 W (●)): (a) atomic copper line at 510.55 nm and (b) atomic copper line at 515.32 nm. The so-called 0 mm position refers to the closest position to the sample surface, which corresponds to a distance of about 9 mm far from the cathode.

A similar analysis was carried out for several copper lines and the results are summarized in Table 5. The distance at which the emission intensity has decreased by 80% in the green plasma regime was estimated for several measurements. Thus, the average distance value over 3 measurements and the corresponding standard deviation obtained are listed in the last column of Table 5. In the violet plasma regime, none of the emission lines of Cu decrease along the plasma plume as much as an 80% of the maximum intensity, which is measured in the 0 mm position. Inspecting the data shown in Table 5 two different trends can be distinguished: the group of lines with upper energy level below 5 eV (the last three lines of the table, including the 510.55 nm line shown in Fig. 4a) presents a decrease to 20% of the emission intensity for distances to the anode longer than 5 mm. Lines with upper energy level above 5 eV (including Cu I 515.32 nm shown in Fig. 4b) show a much faster decrease of the emission intensity. They drop to 20% of their respective maximum value at our reference 0 mm position within the first 4 mm. In conclusion we can say that highly excited states are observed close to the cathode (sample surface). The ionic copper line at 224.70 nm is included in the group of atoms excited to high levels, since the energy of the upper level is 8.23 eV and its emission intensity presents an 80% decrease at a distance of 1.8 mm. No further ionic copper lines could be evaluated due to the low emission intensity registered in the side-on measurements. The excitation temperature, if we can define such a quantity, appears to drop along the plume axis, away from the cathode much faster in the green than in the violet regime.

Fig. 5 displays the ratio of the 324.75 nm and the 510.55 nm lines as a function of the distance from the cathode, for both the green and the violet plasma plume. The fact that this ratio remains constant and consistently higher in the violet plasma indicates that the copper density does not vary much along the plume and is higher in the green plasma plume.

Table 5 Average distance (over 3 measurements) at which the emission intensity of several Cu lines in the green plasma regime has dropped to 20% of its maximum. All the lines correspond to Cu I except for the 224.70 nm line, which corresponds to Cu II. The lines are ordered by the upper energy level

Wavelength/nm	$Energy_{upper\ level}$/eV	Distance where $I = 0.20I_{max}$/mm (from our 0 mm reference position) (green plasma)
224.70 (Cu II)	8.23	1.8 ± 0.3
222.78	7.21	1.8 ± 0.3
368.74	7.18	2.7 ± 0.9
365.42	7.18	2.6 ± 1.0
223.01	6.95	2.0 ± 0.5
515.32	6.19	3.0 ± 0.8
521.82	6.19	2.3 ± 0.3
282.44	5.78	2.5 ± 0.3
222.57	5.57	2.0 ± 0.5
224.43	5.52	1.8 ± 0.3
327.98	5.42	3.4 ± 1.2
333.78	5.10	3.0 ± 0.3
324.75	3.82	5.5 ± 0.6
510.55	3.82	7.0 ± 2.0
327.40	3.79	7.0 ± 2.0

Argon emission. The spatial distribution of Ar I (418.19 nm) emission intensity along the plasma plume axis is shown in Fig. 6. At the 0 mm lateral position similar emission intensity is observed for both plasma regimes. However, a more pronounced

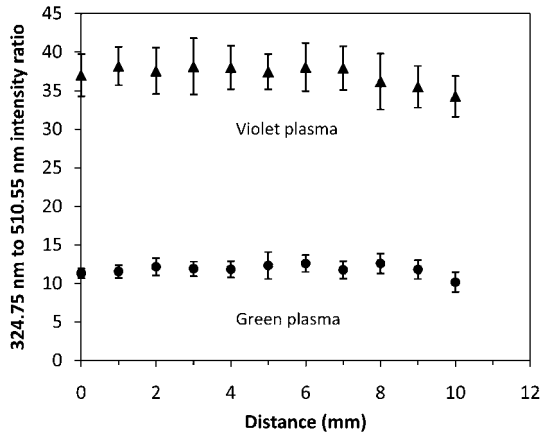

Fig. 5 Relation between the intensity of the 324.75 nm line and the 510.55 nm line, along the plasma plume, for both plasma regimes (violet plasma at 275 sccm, 600 Pa and 40 W (▲); green plasma at 275 sccm, 700 Pa and 40 W (●)).

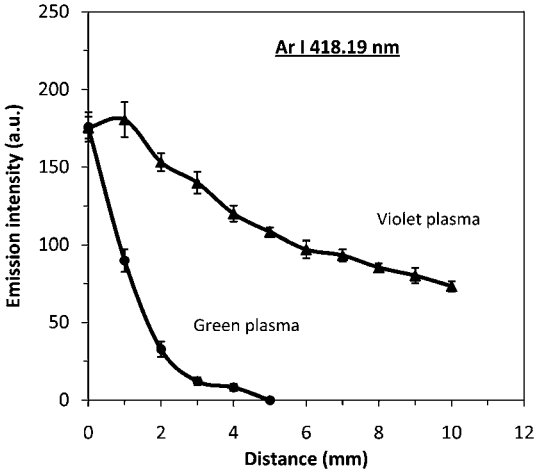

Fig. 6 Spatially resolved measurement of the atomic argon emission at 418.19 nm, for both plasma regimes (violet plasma at 275 sccm, 470 Pa and 40 W (▲); and green plasma at 275 sccm, 600 Pa and 40 W (●)). The so-called 0 mm position refers to the closest position to the sample surface, which corresponds to a distance of about 9 mm far from the cathode.

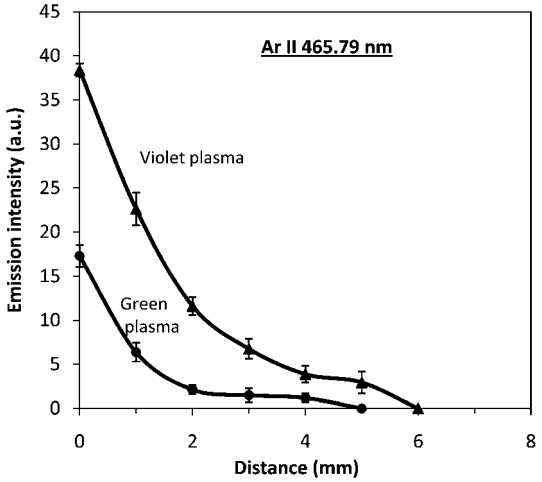

Fig. 7 Spatially resolved measurement of the ionic argon emission at 465.79 nm, for both plasma regimes (violet plasma at 275 sccm, 475 Pa and 40 W (▲); and green plasma at 275 sccm, 600 Pa and 40 W (●)). The so-called 0 mm position refers to the closest position to the sample surface, which corresponds to a distance of about 9 mm far from the cathode.

decrease is observed again for the emission intensity corresponding to the green plasma (the 80% decrease takes place at 2.0 mm in this case, while at a distance of 10 mm in the violet regime the intensity drop is of only 60%). Table 6 summarizes the results of this study extended to different atomic argon lines. In this case it is not possible to distinguish different trends as a function of the energy levels involved in the transition: the green plasma regime shows an 80% decrease of all the studied emission intensities within the first 4 mm of the plasma plume (from our 0 mm reference position), as listed in the last column of Table 6. Moreover, the argon emission intensity in the violet plasma is higher than that measured in the green regime at all the evaluated distances.

The emission distribution of some ionic Ar lines was also studied. Fig. 7 shows the evolution along the plasma plume axis of the emission intensity at 465.79 nm, in the green and violet regimes, respectively. Again the violet plasma shows higher ionic argon emission than the green plasma at all the distances assayed. The intensity decrease is fast for both plasma regimes, although once more the emission is more confined when the plasma is green: the intensity drops to 20% of its maximum at 3.0 mm in the violet plasma and at 1.5 mm in the green plasma. The results obtained for certain selected ionic lines are collected in Table 7. In particular, the distance at which the intensity of the different ionic lines has decreased by 80% was estimated for both plasma regimes. This distance was shorter than 5 mm in the majority of the evaluated cases, being even shorter in the green regime. The observation of ionic lines is interesting on its own, because it indicates that argon ions are still formed in this discharge plume. We should therefore not consider it as a spatial after-glow region.

Table 6 Average distance (over 3 measurements) at which the emission intensity of several Ar I lines in the green plasma regime has dropped to 20% of its maximum. The lines are ordered by the upper energy level

Wavelength/nm	$Energy_{upper\ level}$/eV	Distance where $I = 0.20I_{max}$/mm (from our 0 mm reference position) (green plasma)
418.19	14.69	1.9 ± 0.1
419.83	14.58	1.9 ± 0.1
451.07	14.58	2.4 ± 0.6
415.86	14.53	1.9 ± 0.1
459.61	14.52	2.5 ± 0.5
420.07	14.50	1.9 ± 0.5
470.23	14.46	2.1 ± 0.1
452.23	14.46	2.5 ± 0.5
750.39	13.48	2.5 ± 0.3
751.47	13.27	2.5 ± 0.3
763.51	13.17	3.8 ± 0.3

Table 7 Average distance (over 3 measurements) at which the emission intensity of several Ar II lines has dropped to 20% of its maximum. The lines are ordered by the upper energy level

		Distance where $I = 0.20I_{max}$/mm (from our 0 mm reference position)	
Wavelength/nm	$Energy_{upper\ level}$/eV	Green plasma	Violet plasma
410.39	22.51	—	5.3 ± 0.3
459.88	21.35	2.3 ± 0.3	>10
457.94	19.97	2.5 ± 0.5	3.0 ± 0.3
465.79	19.80	1.6 ± 0.1	3.0 ± 0.3

Conclusions

A new experimental set-up has been developed to achieve spatially resolved optical emission measurements in a radio-frequency glow discharge, provided with a modified Grimm-type analytical source. Two different plasma regimes, defined as green and violet plasma, have been observed and characterized using

a pure copper sample cathode. Keeping the same Ar flow rate, the violet regime is established at pressures lower than a certain threshold and shows higher Ar emission and a further expansion of the plasma plume. Additionally, the resonance Cu emission lines are less affected by self-absorption. On the other hand, at higher pressures above the threshold, the plasma takes a green color which corresponds to an enhancement of Cu emission, and presents a more confined emission within the proximity of the anode. The condition for transition between the two plasma regimes is not well defined. It is not yet understood what actually triggers the switching from one mode to the other.

Although the difference in the emission characteristics between the green and violet plume is significant, the differences are minor when observed end-on. In end-on view, most of the observed radiation originates from the discharge area close to the cathode, the brightest part of the discharge. The sputtering rates in the green and violet plasma are not sufficiently different to explain the higher Cu emission (and self-absorption) in the green plume. The major difference between these regimes must, therefore, be related to transport of material, away from the cathode.

These differences between the end-on and side-on views are important to the interpretation of GD-MS results. Contrary to GD-OES, transport of matter from the sample to the sampler orifice plays a crucial role in the signal generation in GD-MS. Whereas in GD-OES photon emission and detection are dominated by the brightest area close to the cathode, ions detected by the mass spectrometer of the GD-MS system originate from the vicinity of the sampler orifice. Moreover, as the highly excited species and ions drop quickly away from the cathode, the spatial position of the sampler in the MS instruments should be reconsidered and placed closer to the cathode.

Acknowledgements

The authors gratefully acknowledge financial support by EU through the Marie Curie Research Training Network GLADNET (MRTN-CT-2006-035459) and the STREP project EMDPA (STRP 032202); and by the Spanish Ministry of Science and Innovation, and FEDER Programme through the project MAT2007-65097-C02. R. Valledor acknowledges financial support by the Spanish Ministry of Education (Ph.D. "FPU" Grant). J. Pisonero acknowledges financial support from "Ramón y Cajal" Research Program of the Spanish Ministry of Education, cofinanced by the European Social Fund.

References

1 M. R. Winchester and R. Payling, *Spectrochim. Acta, Part B*, 2004, **59**, 607–666.
2 J. Pisonero, B. Fernandez, R. Pereiro, N. Bordel and A. Sanz-Medel, *TrAC, Trends Anal. Chem.*, 2006, **25**, 11–18.
3 J. Pisonero, *Anal. Bioanal. Chem.*, 2006, **384**, 47–49.
4 T. Nelis and J. Pallosi, *Appl. Spectrosc. Rev.*, 2006, **41**, 227–258.
5 M. Guilhaus, D. Selby and V. Mlynski, *Mass Spectrom. Rev.*, 2000, **19**, 65–107.
6 R. Valledor, J. Pisonero, N. Bordel, J. I. Martin, C. Quiros, A. Tempez and A. Sanz-Medel, *Anal. Bioanal. Chem.*, 2010, **396**, 2881–2887.
7 Y. Zenitani and K. Wagatsuma, *Anal. Sci.*, 2008, **24**, 555–557.
8 G. Gamez, S. J. Ray, F. J. Andrade, M. R. Webb and G. M. Hieftje, *Anal. Chem.*, 2007, **79**, 1317–1326.
9 M. Dogan, K. Laqua and H. Massmann, *Spectrochim. Acta, Part B*, 1971, **26**, 631–649.
10 K. Hoppstock and W. W. Harrison, *Anal. Chem.*, 1995, **67**, 3167–3171.
11 K. Rozsa, A. Gallagher and Z. Donko, *Phys. Rev. E: Stat. Phys., Plasmas, Fluids, Relat. Interdiscip. Top.*, 1995, **52**, 913–918.
12 G. P. Jackson, C. L. Lewis, S. K. Doorn, V. Majidi and F. L. King, *Spectrochim. Acta, Part B*, 2001, **56**, 2449–2464.
13 C. L. Lewis, G. P. Jackson, S. K. Doorn, V. Majidi and F. L. King, *Spectrochim. Acta, Part B*, 2001, **56**, 487–501.
14 R. K. Marcus, *Glow Discharge Spectroscopies*, Plenum Press, New York, 1993.
15 P. Smid, E. B. M. Steers and V. Hoffmann, *24th Summer School and International Symposium on the Physics of Ionized Gases, Contributed Papers*, 2008, pp. 325–329.
16 J. Pisonero, J. M. Costa, R. Pereiro, N. Bordel and A. Sanz-Medel, *J. Anal. At. Spectrom.*, 2001, **16**, 1253–1258.
17 J. Pisonero-Castro, J. M. Costa-Fernandez, R. Pereiro, N. Bordel and A. Sanz-Medel, *J. Anal. At. Spectrom.*, 2002, **17**, 786–789.
18 A. C. Muniz, J. Pisonero, L. Lobo, C. Gonzalez, N. Bordel, R. Pereiro, A. Tempez, P. Chapon, N. Tuccitto, A. Licciardello and A. Sanz-Medel, *J. Anal. At. Spectrom.*, 2008, **23**, 1239–1246.
19 T. Nelis, M. Aeberhard, L. Rohr, J. Michler, P. Belenguer, P. Guillot and L. Therese, *Anal. Bioanal. Chem.*, 2007, **389**, 763–767.
20 http://www.nist.gov/physlab/data/asd.cfm.
21 R. Payling and P. L. Larkins, *Optical emission lines of the elements*, John Wiley and Sons Ltd, 1999.
22 A. Martin, A. Martinez, R. Pereiro, N. Bordel and A. Sanz-Medel, *Spectrochim. Acta, Part B*, 2007, **62**, 1263–1268.
23 A. Bengtson and T. Nelis, *Anal. Bioanal. Chem.*, 2006, **385**, 568–585.